# ARTICLES

## Spin−Orbit and Vibrational Relaxation Rate Constants and Radiative Lifetimes for $v'=0-5$ Levels of PF($A^3\Pi_{0,1,2}$) Molecules†

**Boris Nizamov‡ and D. W. Setser***

*Department of Chemistry, Kansas State University, Manhattan, Kansas 66502*

*Received: September 27, 2001; In Final Form: January 14, 2002*

One-photon laser excitation of PF($X^3\Sigma^-$) molecules generated in a discharge-flow reactor was used to prepare PF($A^3\Pi_{0,1,2}$) molecules in selected vibrational and spin−orbit levels. The radiative lifetimes, collisional relaxational mechanisms, and state-to-state rate constants for spin−orbit and vibrational relaxation were assigned in He and Ar bath gas for $v'=0-5$ levels at 300 K. The radiative lifetimes, which are independent of the spin−orbit quantum number, $\Omega$, decrease from 4.2 to 1.8 $\mu$s for $v'=0-5$. The spin−orbit relaxation mechanisms in He and in Ar are independent of $v'$ level to within the experimental uncertainty. However, the actual rate constants for spin−orbit relaxation are different in He and Ar. In He the rate constant for $\Delta\Omega=-2$ change are 2-fold larger than those for $\Delta\Omega=-1$, whereas in Ar the order is reversed and the rate constants for $\Delta\Omega=-1$ change are larger than the rate constant for $\Delta\Omega=-2$ change. Furthermore, in Ar the rate constant for $\Delta\Omega=-1$ transfer is much larger for $^3\Pi_1\rightarrow{}^3\Pi_0$ than for $^3\Pi_2\rightarrow{}^3\Pi_1$. Although the vibrational relaxation mechanisms in He and Ar have different degrees of involvement of the spin−orbit states, the overall vibrational deactivation rate constants are similar in He and Ar and both increase with vibrational level.

### Introduction

The metastable $a^1\Delta$ states of the diatomic molecules that are isovalent with $O_2$ have been investigated extensively because of their promise as gas phase, energy storage systems.[1,2] The $O_2$ ($a^1\Delta$), NF ($a^1\Delta$), and NCl ($a^1\Delta$) molecules are especially useful because large concentrations can be generated chemically.[3−5] In principle, the PF molecule also could be an interesting energy storage system, and it has the added advantage, relative to NF and NCl, that the PF($A^3\Pi_{0,1,2}$) and PF($d^1\Pi$) states (with the $\sigma^2\pi^4\pi^{*1}\sigma^{*1}$ configuration) are bound and facilitate monitoring of PF($X^3\Sigma^-$) and PF($a^1\Delta$) concentrations by laser-induced fluorescence. These PF($A^3\Pi_{0,1,2}$ and $d^1\Pi$) states, which have lifetimes of 4 and 1 $\mu$s, respectively, could themselves be laser candidates. Unfortunately, as for the isovalent SO($A^3\Pi$) state,[6−8] the PF($A^3\Pi$ and $d^1\Pi$) states are readily quenched[9] and practical applications seem unlikely, even though an energy-pooling reaction between PF($b^1\Sigma^+$) and NF($b^1\Sigma^+$) giving PF($A^3\Pi$) was discovered.[10] Another unsolved problem is the chemical generation of high concentrations of PF($b^1\Sigma^+$ or $a^1\Delta$) molecules.[11] As the final part of a program[9−13] to investigate the PF chemical system, we now wish to report a study of the spin−orbit relaxation of the PF($A^3\Pi_{0,1,2}$) states for $v'=0-4$ and vibrational relaxation for $v'=1-5$ in He and Ar at 300 K. The radiative lifetimes of the $v'=0-5$ levels also were measured. These data augment our earlier report[9] of the spin−orbit relaxation mechanism for PF($A^3\Pi_{0,1,2}$),$v'=0$. The electronic quenching rates for PF($A^3\Pi$) by He and Ar are negligibly small for the pressures used here, and electronic quenching does not need to be considered.[9]

The PF($A^3\Pi_{0,1,2}$) molecule provides a convenient case for assignment of rate constants for collisional relaxation among the $^3\Pi_0(F_1)$, $^3\Pi_1(F_2)$P, and $^3\Pi_2(F_3)$ spin−orbit states, which are separated by about 142 cm$^{-1}$. The PF(A) state is a good example of Hund's case (a) coupling, since the spin−orbit constant ($A$=142 cm$^{-1}$) is much larger than the rotational constant (0.45 cm$^{-1}$).[13] Populations in individual spin−orbit states can be prepared by one-photon absorption from PF($X^3\Sigma^-$,$v''=0$) molecules, which are conveniently generated in a discharge-flow reactor.[9] The PF(A→X) fluorescence can be resolved with a monochromator and collisional transfer to lower vibrational levels and/or transfer to spin−orbit states of the same or lower vibrational level can be observed as a function of He or Ar pressures, which serve as carrier gases in the flow reactor. The rotational relaxation rates are sufficiently rapid that the initially prepared spin−orbit state attains a thermal rotational distribution before spin−orbit relaxation occurs.[14] Thus, no information about final rotational or Λ-doublet states from the spin−orbit transfer event can be deduced from the present experiments, and the question of formation of high rotational states with minimization of the translational energy defect[15] in the $\Delta\Omega = -1$ or $-2$ processes cannot be directly answered. On the other hand, the role of the spin−orbit states in the vibrational relaxation mechanism of PF($A^3\Pi$,$v'\geq 1$) molecules, $\omega_e = 436$ cm$^{-1}$ can be investigated. As illustrated in Figure 1, the $^3\Pi_0$ level of the $v'+1$ state is ∼150 cm$^{-1}$ above the $^3\Pi_2(v')$ level. Thus, vibrational relaxation can proceed with conservation of $\Omega$ with a large energy defect or by change in $\Omega$ with a smaller energy defect. As shown in Figure 1, five rate

† Part of the special issue "Donald Setser Festschrift".

‡ Current address: Department of Chemistry, Johns Hopkins University, 3400 N. Charles Street, Baltimore, Maryland 21218.

10.1021/jp013632w CCC: $22.00 
Published on Web 03/09/2002

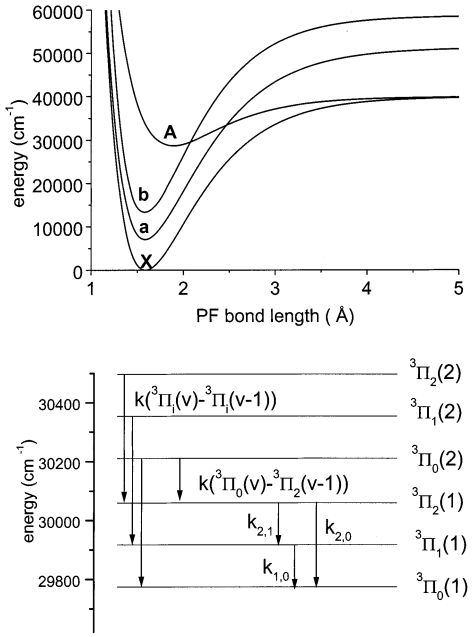


**Figure 1.** Schematic representation of the spin−orbit and vibrational levels of PF(A$^3\Pi$) with definition of the rate constants used in the model for collisional relaxation. The energy separation between the spin−orbit levels is 142 cm$^{-1}$ and the separation between the $^3\Pi_0(v')$ and $^3\Pi_2(v'-1)$ levels is 152 cm$^{-1}$.The potentials for the PF(X$^3\Sigma^-$, a$^1\Delta$, b$^1\Sigma^+$ and A$^3\Pi$) states are also shown.

constants were used to describe the relaxation for each vibrational level; these are the purely spin−orbit relaxation rate constants, $k^v_{2,1}$, $k^v_{2,0}$, and $k^v_{1,0}$, plus the vibrational relaxation rate constants, $k(^3\Pi_i(v')\rightarrow{}^3\Pi_i(v'-1))$, without change in $\Omega$ and vibrational relaxation from the $\Omega=0$ state to the nearest $v'-1$ state, $k(^3\Pi_0(v')\rightarrow{}^3\Pi_2(v'\text{-}1))$. The $k(^3\Pi_i(v\Pi') \rightarrow {}^3\Pi_i(v'-1))$ values for $i = 0$, 1, and 2 were assumed to be equal; the other $\Delta v'=-1$ processes with $\Delta\Omega\neq0$ were assumed to be negligible because of the larger energy defects. The rate constants for reverse processes are determined by detailed balance; thus $k(^3\Pi_2(v')\rightarrow(^3\Pi_0(v'+1))$ is determined by analysis of the relaxation of the $^3\Pi_0(v'+1)$ level.

According to a model based on first-order perturbation theory[16] with an interaction potential between PF(A) and He or Ar determined by electrostatic forces, a direct coupling exists between the $\Omega = 0$ and 2 states. In the first-order perturbation limit, the component of the electron spin angular momentum, $\Sigma(h/2\pi)$, that is coupled to the PF internuclear axis should not change during a collision.[16−19] Therefore, the transfer of population between the $\Omega = 2$ and 0 states by collisional reorientation of the orbital angular momentum, $\Lambda(h/2\pi)$, should have a faster rate than the transfer of population from $\Omega=2$ to $\Omega=1$ or from $\Omega=1$ to $\Omega = 0$ or 2. Although experimental data for $^3\Pi_{0,1,2}$ molecules with fully developed case (a) coupling are scarce, results for PF(A$^3\Pi$,$v'=0$),[9] SO(A$^3\Pi$,$v'=0$),[6−8] and PH(A$^3\Pi$,$v'=0$)[18] suggest that the above prediction is not rigorously followed even for collisions with He. For molecules such as NH(A$^3\Pi$)[19] and PH(A$^3\Pi$)[18], the change from case (a) coupling for low $J$ rotational levels to case (b) for higher rotational levels complicates use of the propensity rules that might be appropriate for strict Hund's case (a) or (b) coupling. The mixing of the case (a) basis set wave functions for PF(A) is less than 3% for $N=35$. Thus, the PF(A$^3\Pi$) molecule is adequately described by Hund's case (a) coupling for the whole range of rotational levels ($N\leq35$) populated at room temperature, and it provides a good test of the propensity rules for $^3\Pi$-state molecules with Hund's case (a) typing coupling. The present study refines the rate constants previously published for PF(A$^3\Pi$,$v'=0$)[9] and extends the results up to $v'=4$ for He and $v'=5$ for Ar. Within the experimental uncertainty, the spin−orbit relaxation mechanism does not depend on vibrational level. Since the vibrational relaxation rates in He and Ar are ~5 times slower than the spin−orbit relaxation rates, the role of the spin−orbit states in the vibrational relaxation mechanism could be characterized. The model for $\Delta v'=-1$ relaxation includes processes that conserve the $\Omega$ quantum number plus processes that transfer population from $^3\Pi_0(v')$ to $^3\Pi_2(v'-1)$ levels. It was not necessary to include vibrational relaxation steps with $\Delta\Omega=\pm1$ changes, but the present experiments do not necessarily exclude small rate constants for those processes.

## Experimental Methods

The experimental results to be reported were obtained with the same apparatus that was described in detail in ref 9. The PF(X$^3\Sigma^-$) concentration was generated by passing a flow of $PF_3$ in He or in Ar through a microwave powered discharge. The PF(A$^3\Pi$) molecules were excited to selected $v'$ and $\Omega$ states by the frequency-doubled output of the Lambda Phyzik dye laser pumped by a 10 Hz YAG laser. For the desired wavelength range (341−335 nm), the pulse energy was typically 1−2 mJ with a pulse duration of 10 ns and a bandwidth of 0.4 cm$^{-1}$. The PF(A) fluorescence was observed with a 1 m monochromator fitted with a 500 nm blazed grating (1200 lines mm), usually used in the second order, and a Hamamatsu R-955 photomultiplier tube. The variation of the response of the detection system with wavelength was calibrated with standard deuterium or quartz−iodine lamps. In most experiments the excitation wavelength was chosen to give the maximum fluorescence signal. For a A$^3\Pi_{0,1,2}\leftarrow$X$^3\Sigma^-$ transition, the $F_3$ and $F_1$ components have nine rotational branches and the $F_2$ component only six branches. Therefore, different features were used as excitation wavelengths for the $F_1$, $F_2$, and $F_3$ components. Examples of typical excitation spectra can be found in refs 9 and 13. For excitation of the $F_2$ component, the laser wavelength was chosen to be the same as the wavelength of the bandhead of the $R_{21}$ rotational branch. With this choice of excitation wavelength and for a laser bandwidth of 0.4 cm$^{-1}$, the number of rotational levels prepared by a laser pulse is less than five and centered at $J'\sim9$. The value of $J'$ at which the $R_{21}$ bandhead is formed slowly decreases as $v'$ increases. For the $F_3$ and $F_1$ components, the excitation wavelengths were chosen to be close to the wavelengths of the $R_{32}$ and $R_{12}$ bandheads, respectively, usually slightly to the red from these features. In this case, rotational levels with $J'<6$ are excited. Since B″(0)−B′($v'$) changes with $v'$, the laser wavelength can accidently overlap rotational lines from the $R_1$ and $Q_1$ branches, in which case one or two rotational levels with high $J'$ were prepared in addition to the range of rotational levels with $J'<6$. Although only low rotationally levels were initially excited, full rotational relaxation ($N_{mp}=15$ at 300 K) was verified by observing the development of the shape of the emission bands[14] from a given $v'$, $\Omega$ level from spectra acquired with different time gates. Except for the $k_{1,0}$ values in Ar, vide infra, the rotational relaxation rates within a given $\Omega$ state are an order of magnitude faster than the spin−orbit or vibrational relaxation rates.

The time-resolved data consist of decay profiles from the initially prepared PF($^3\Pi_\Omega$,$v'$) level plus growth and decay profiles of individual product levels for various He and Ar pressures. A time profile normally could be acquired with 1000 laser pulses. Additional data consisted of time-integrated

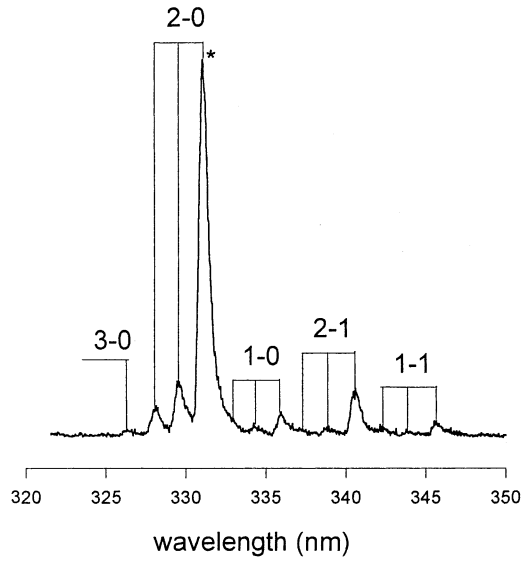


**Figure 2.** Integrated fluorescence spectrum following excitation of PF($A^3\Pi_0, v'=2$) in 1 Torr of He. The majority of the fluorescence from $v'=2$ is to $v''=0$. Note the small degree of spin−orbit and vibrational relaxation at 1 Torr of He.

fluorescence spectra acquired at different pressures. The integrated fluorescence intensities of the individual $v''$ bands from a given $^3\Pi_\Omega, v'$ level were converted to relative concentrations using the appropriate radiative branching fractions.[13]

The signal from the photomultiplier tube was recorded with a Hewlett-Packard digital scope (500 MHz). The waveforms were transformed to a computer and stored. Fluorescence spectra were obtained by slowly scanning the monochromator with integration of the waveforms, as the laser provided constant energy pulses. Some integrated fluorescence spectra (typically with a 0−10 $\mu$s time gate) from excitation of $v'=2$ for several pressures of He are shown in Figures 2 and 3. The strongest band in the $v''$ progressions always is to $v''=0$. The typical resolution of the monochromator was 0.4−0.8 nm.

## Experimental Results

**A. Radiative Lifetimes and Overall Vibrational Relaxation Rate Constants in He and Ar.** Radiative lifetimes were measured for a 300 K Boltzmann distribution of rotational levels of a given $v'$, $\Omega$ state, because the rotational relaxation rate is faster than spin−orbit and vibrational relaxation rates, as discussed in the Experimental Section. The rate constants of the reverse processes were fixed using the detailed-balance principle. The energy gap between the spin−orbit states was taken as the spin−orbit constant, which is ~142 $cm^{-1}$. We neglected the fact that $J=0$ level does not exist for $\Omega=1$ and $J=0$ and 1 levels do not exist for $\Omega=2$. Considering the relatively large number of populated rotational levels at 300 K, ignoring the absence of these three rotational levels is not serious. The detailed balance principle gives the ratio of constants for $^3\Pi_2 \rightleftarrows {}^3\Pi_1$ and $^3\Pi_1 \rightleftarrows {}^3\Pi_0$ as 0.51 and 0.48 for $^3\Pi_2(v'+1) \rightleftarrows {}^3\Pi_0$ ($v'$). Stated in another way, the ratio of equilibrium populations in adjacent levels shown in Figure 1 should be approximately 0.5 at room temperature.

An experiment was done to confirm the lifetime reported in ref 9 for $v'=0$. The emission from excitation of the $^3\Pi_0(v'=0)$ state at 2.0 Torr of Ar was collected using a band-pass filter that passed the fluorescence from all three spin−orbit states. This waveform represents radiative decay of the total population, since electronic quenching is negligible at this pressure and

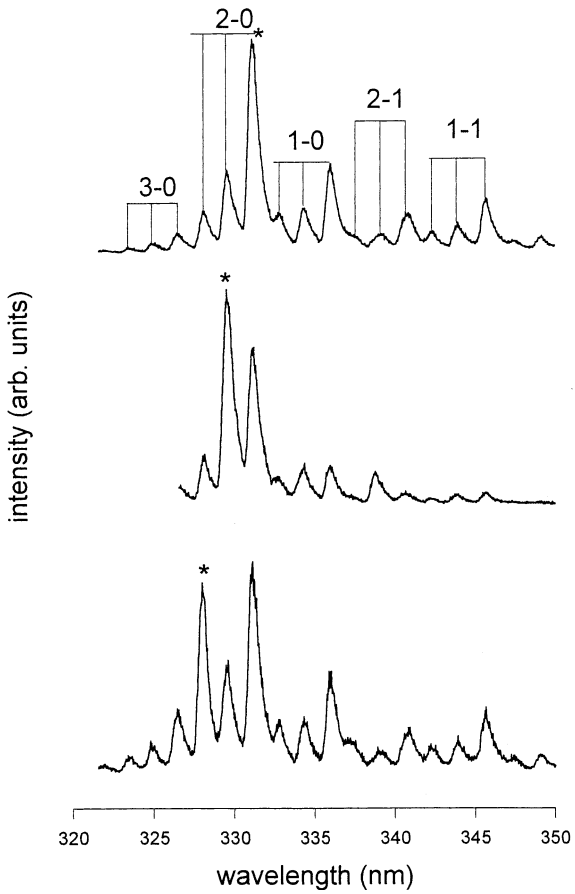


**Figure 3.** Representative integrated fluorescence spectra at 4 Torr pressure of He following excitation of the $^3\Pi_0$, $^3\Pi_1$ and $^3\Pi_2$ levels for $v'=2$. The asterisk denotes the band that was utilized for excitation by the laser. Both vibrational and spin−orbit state relaxation are evident at 4 Torr of He.

vibrational relaxation can be neglected. The slope of the semilogarithmic plot of the decay waveform gave a decay lifetime of 4.2 ± 0.2 $\mu$s, which is in excellent agreement with the result from ref 9.

Radiative lifetimes for $v'>0$ levels were measured using three different methods. Direct determination of the radiative lifetimes from very low-pressure experiments, where the sum of the first-order relaxation rate constants are much smaller than the radiative rate constant, was attempted. Experiments were limited to pressures >0.3 Torr of Ar or He carrier gas because the microwave discharge was unstable at lower pressures. Emission spectra for $v'=2-5$ collected at 1.0 Torr of He, see Figure 2, showed that the extent of spin−orbit and vibrational relaxation was small, confirming that most of the population in the initially prepared level decays radiatively at this pressure. Waveforms from excitation of the $^3\Pi_0(v'=1-5)$ states with observation of the fluorescence from the same initial state via the monochromator were collected at 0.3 Torr, and decay rate constants calculated using these waveforms were used as the first approximation for the radiative decay rate constants in the initial fitting of the ratio of relative emission intensities. After spin−orbit rate constants were assigned, the radiative decay rate constants were recalculated and the iteration repeated. This was a fast converging process, since the initial approximation for the radiative rate constant from the waveforms collected at 0.3 Torr is already within 80−85% of its true value. Experiments also were done with excitation of $^3\Pi_2(v')$ and $^3\Pi_1(v')$ in He at 0.3 Torr to show that the radiative lifetimes were independent of $\Omega$.

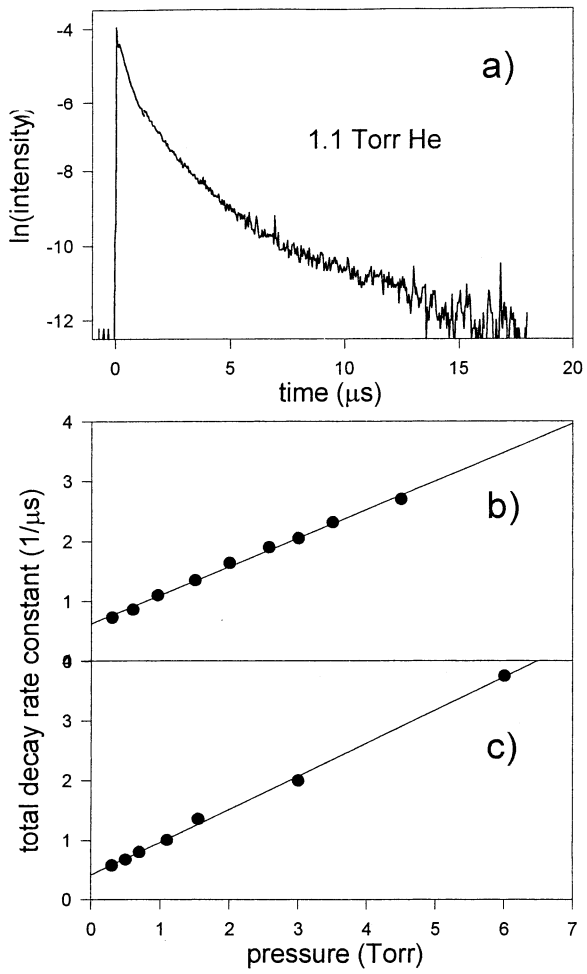


**Figure 4.** Total decay constants of PF($A^3\Pi_2$,$v'$ = 2 and 4). (a) A representative waveform, on a logarithmic scale, for the decay of PF($A^3\Pi_2$,$v'$=2) in 1.1 Torr of He. The total first-order loss of population from $^3\Pi_2$,$v'$=2 was obtained by fitting the 0−1 $\mu$s part of the waveform. (b) Stern−Volmer plot of the short-time, decay constants of PF($A^3\Pi_2$, $v'$ = 2) vs He pressure. (c) Stern−Volmer plot of the short-time decay constants of PF($A^3\Pi_2$,$v'$=4) vs He pressure. The slopes and intercepts of these plots give the total relaxation rate constants and the radiative lifetimes, respectively.

In the second approach, waveforms from excitation of the $^3\Pi_2$($v'$=2−4) states with observation of the fluorescence from the initial, $\Omega$ = 2 state via the monochromator were collected at different pressures. The initial part of the decay waveforms was used to determine the total removal rate constants; see Figure 4a. These total removal rate constants were plotted vs pressure and the intercept of this plot was taken as the radiative decay rate constant of a given vibrational level. Some typical data are shown in Figure 4b, and the $k^{He}_{tot}$ values for the $^3\Pi_2$ states are listed in Table 1. These experiments were not done with Ar.

Radiative lifetimes and overall vibrational relaxation rate constants were obtained by analyzing the decay waveforms in the time domain where the three spin−orbit states were collisionally coupled. For excitation of $v'$>1, vibrational relaxation can be considered irreversible because of the large pool of states below the initially prepared level, and because the reverse processes are endothermic and hence have smaller rate constants. Since the vibrational relaxation was considered to be irreversible, the kinetics of the spin−orbit relaxation was described by a system of first-order linear differential equations. Solutions of these equations are linear combinations of exponential terms with decay constants, $\lambda_1$, $\lambda_2$, and $\lambda_3$, which are eigenvalues of the corresponding rate matrix. One of these decay constants, which we arbitrarily chose to be $\lambda_3$, is significantly smaller than the other two, and it is the rate constant for the decay of the total $^3\Pi_2$, $^3\Pi_1$, and $^3\Pi_0$ population in a given $v'$ level. For times longer than $\lambda_1 t$ and $\lambda_2 t$ >1, only the slow component survives, and $\lambda_3$ can be found from the analysis of waveforms for these longer times. In this limit, the slopes of the semilogarithmic plot of the $^3\Pi_{0,1,2}$ waveforms from excitation of any of the $^3\Pi_{0,1,2}$ initial states are the same and equal to $\lambda_3$, e.g., the populations in the spin−orbit states have their equilibrium values as shown in Figure 5a. The intercept of the plot of the $\lambda_3$ values vs pressure gives the radiative lifetime, see Figure 5b. The radiative lifetimes measured by the three methods for $v'$=2 were 2.7, 2.5, and 2.4 $\mu$s. Radiative lifetimes determined by all three methods were in good agreement; however, the low-pressure measurement is the most direct, and these are the recommended lifetimes listed in Table 1.

**TABLE 1: Radiative Lifetimes, Overall Vibrational Deactivation Rate Constants and Total quenching constants[a,b] (in He) for PF($A^3\Pi$)**

| vibrational level | $\tau^c$ ($\mu$s) | $k^{He}_{vib}$ | $k^{He}_{tot}$ | $k^{Ar}_{vib}$ |
|---|---|---|---|---|
| 0 | 4.2 ± 0.2 | | | |
| 1 | 3.2 ± 0.2 | 1.5 ± 0.2[d] | | 1.4 ± 0.2[d] |
| 2 | 2.7 ± 0.2 | 2.2 ± 0.3 | 15 ± 1 | 3.1 ± 0.2 |
| 3 | 2.4 ± 0.1 | 3.2 ± 0.5 | 17 ± 2 | |
| 4 | 2.0 ± 0.1 | 3.6 ± 0.5 | 19 ± 2 | 3.9 ± 0.5[e] |
| 5 | 1.8 ± 0.1 | | | 6.1 ± 1.0 |

[a] In units of $10^{-12}$ cm$^3$ molecule$^{-1}$ s$^{-1}$. [b] The total relaxation rate constant is the sum of $k^{He}_{vib}$ + $k^{He}_{2,1}$ + $k^{He}_{2,0}$ for $^3\Pi_2$($v'$) states. [c] The radiative lifetimes are the same for the three $\Omega$ states of the same $v'$ level. [d] Results from ref 9; however, these values for the rate constants were confirmed in the present work. [e] Although this was the value obtained from the Stern−Volmer plot, the fitting of the state-resolved vibrational relaxation data favored a larger value for $k^{Ar}_{vib}$.

To obtain more reliable values of the slopes for the $\lambda_3$ vs pressure plots, zero pressure intercepts corresponding to the best radiative lifetimes were added to the Stern−Volmer plots, such as shown in Figure 5b. The slope of the $\lambda_3$ vs pressure plots provide the overall rate constants for vibrational relaxation, and these values are given in Table 1 as $k^{He}_{vib}$ and $k^{Ar}_{vib}$. These rate constants for vibrational relaxation do increase with $v'$, and the values for He and Ar are similar. The $k^{v}_{tot}$ values in Table 1 can be compared to $k^{v}_{vib}$ values for He. The difference between $k^{v}_{tot}$ and $k^{v}_{vib}$ provide a rough measure of $k_{2,1}$+$k_{2,0}$, since the rate constant for electronic quenching is negligible.

**B.1. Spin−Orbit and State-Resolved Vibrational Relaxation Rate Constants in He.** Analysis of the data given in ref 9 was repeated to confirm the mechanism and rate constants assigned to spin−orbit relaxation for $v'$=0. For this level, vibrational relaxation can be neglected because collisional excitation to $v'$=1 is endoergic and attention can be focused on just $k_{2,0}$, $k_{2,1}$, and $k_{1,0}$. In the present analysis, the pressure dependence of the ratio of the concentrations in the $^3\Pi_0$, $^3\Pi_1$, and $^3\Pi_2$ levels was used together with the time dependent data to assign the rate constants. The $k_{2,1}$, $k_{2,0}$, and $k_{1,0}$ values, which are given in Table 2, confirm the basic mechanism assigned previously.[9] However, the $k_{1,0} = 0.80 \times 10^{-11}$ value is preferred rather than previous assignment of $0.50 \times 10^{-11}$ cm$^3$ s$^{-1}$. The 2-fold larger value for $k_{1,0}$ vs $k_{2,1}$ is a real difference, which should be noted.

Following the refinement of the rate constants for $v'$=0, a comprehensive effort[14] was made to study the spin−orbit relaxation of $v'$=2. Two types of measurements were made to determine the rate constants. Emission spectra from excitation of each of the spin−orbit states were collected for He pressures

**TABLE 2: Spin−Orbit Relaxation Rate Constants for PF($A^3\Pi$)**

| | He[b] | | | Ar[c] | | |
|---|---|---|---|---|---|---|
| vibrational level | $k_{2,0}$ | $k_{2,1}$ | $k_{1,0}$ | $k_{2,0}$ | $k_{2,1}$ | $k_{1,0}$ |
| 0[b,c] | 1.0 + 0.2 | 0.40 ± 0.08 | 0.80 ± 0.16 | 0.50 ± 0.8 | 1.2 ± 0.2 | 8.0 ± 1.2 |
| 1 | | not measured | | | not measured | |
| 2 | 0.80 ± 0.16 | 0.32 ± 0.06 | 0.80 ± 0.16 | 0.40 ± 0.10 | 1.2 ± 0.2 | 6.0 ± 2.0 |
| 3 | 1.0 ± 0.3 | 0.35 ± 0.10 | 0.80 ± 0.24 | | not measured | |
| 4 | 1.2 ± 0.3 | 0.40 ± 0.12 | 0.80 ± 0.24 | 0.30 ± 0.10 | 1.3 ± 0.1 | 8.0 ± 2.0 |
| 5 | | not measured | | not measured | | 7.0 ± 2.1 |

[a] The units of the rate constants are $10^{-11}$ cm$^3$ molecule$^{-1}$ s$^{-1}$; the values for the reverse rate constants were determined by detailed balance, which is a factor of 0.51 at 300 K. [b] These values for $v'=0$ in He are consistent with the assignments given in ref 9. [c] The $k_{2,0}$ and $k_{2,1}$ values in Ar are consistent with the assignments given in ref 9; however, the $k_{1,0}$ value in Ar is much larger than the previous estimate (see text for explanation).

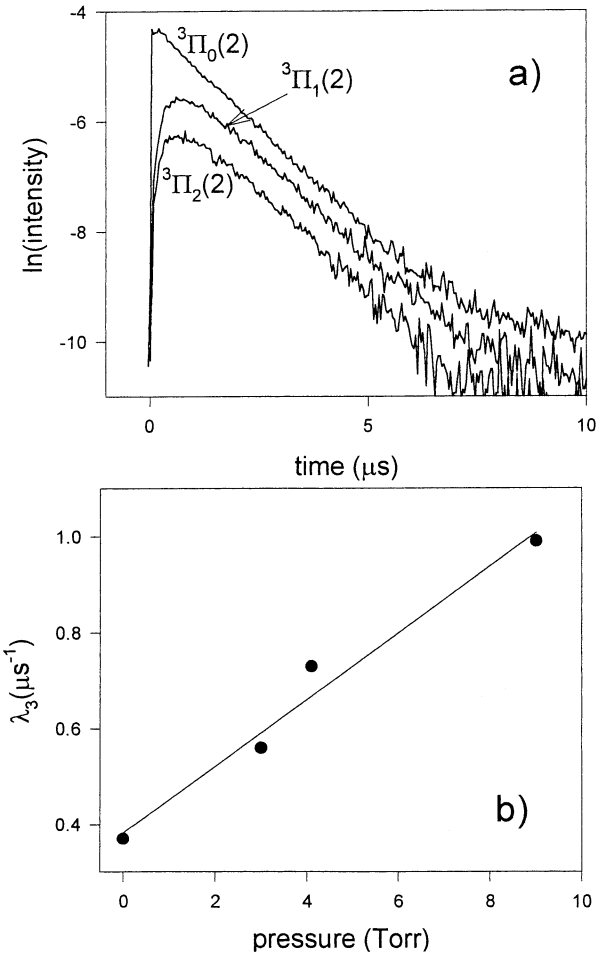


**Figure 5.** Total vibrational relaxation rate constant for PF(A,$v'=2$) in He. (a) Waveforms, on a logarithmic scale, for the decay of the PF($A^3\Pi_{0,1,2}$,$v'=2$) levels following excitation of $^3\Pi_0$,$v'=2$ in 4.1 Torr of He. Note that the spin−orbit states have reached their equilibrium concentrations after 2 $\mu$s. (b) Stern−Volmer plot of the long-time decay constants, obtained from data such as shown in the top part, vs He pressure. The point at zero pressure, which is the $\tau^{-1}_{v'=2}$ value from Table 1, was added to better define the slope of the plot. The extrapolation to estimate $\tau^{-1}_v$ was made without this added point.

of 1 to 4 Torr with an integration time of 0−10 $\mu$s. These spectra were augmented by time-resolved observation following excitation of the individual $\Omega = 0$, 1, and 2 levels with measurement of the growth and decay of the populations in the two other levels and decay from the parent level. The mechanism required both $\Delta\Omega = 1$ and 2 rates and the best values for $k_{2,0}$, $k_{2,1}$, and $k_{1,0}$ were nearly the same as for $v'=0$. Less extensive experiments were done for $v' = 3$ and 4, which confirmed that the spin−orbit relaxation mechanism was invariant with vibrational level. The assigned rate constants for $v'=0-4$ are summarized in Table 2, and the methodology used for analysis of the $v'=2$ data is described in more detail below.

Assignment of the spin−orbit rate constants for $v'>0$ had to be done simultaneously with consideration of the vibrational relaxation rate constants, since the vibrational relaxation rates are not negligible compared to the spin−orbit relaxation rates, as illustrated by the spectra in Figures 2 and 3. The total vibrational relaxation rate constant, $k_{vib}^{He}(2)$, was obtained by analysis of the decay of collisionally coupled spin−orbit states, as described in section A. These $k_{vib}^{He}(v)$ values are the Boltzmann average effective rate constant for the three $^3\Pi_{0,1,2}$ levels. As a first approximation, it was assumed that removal of the population from a given spin−orbit state due to vibrational relaxation does not depend on $\Omega$. In this approximation, we replaced radiative decay rate constants by the experimentally measured values of $\lambda_3 = \tau_v^{-1} + [He]k_{vib}^{He}(v)$ and then obtained spin−orbit relaxation rate constants by simulation of the relative band intensities for the $^3\Pi_{2,1,0}$ levels for various pressures following excitation of the individual levels; see Figure 3 for sample spectra. As the final check, kinetic simulations of the waveforms following excitation of $^3\Pi_2$ and $^3\Pi_1$ were made. Fits to such data for $v'=2$ are illustrated in Figure 6. Based upon the extensive data set for $v'=2$ in He, which included many integrated spectra plus time-resolved growth and decay measurements, we believe that the spin−orbit rate constants for $v'=2$ are good to ± 20%. The most important conclusion is that both the mechanism and the spin−orbit rate constants for $v'=2$ are nearly the same as those for $v'=0$. The analysis[14] of the data for $v' = 3$ and 4 followed the same procedure as described for $v'=2$. Since the number of spectra and waveforms was less than for $v'=2$, the uncertainty in the rate constants in the Table 2 is estimated as ±30%. For each vibrational level, the $k_{2,0}$ and $k_{1,0}$ rate constants are nearly equal and $k_{1,0}/k_{2,1} \sim 2$.

The last step in the analysis of the $v'=2$ data was to develop a state-resolved model for vibrational relaxation. Spectra obtained at 1−3 Torr, see Figures 2 and 3, for excitation of $^3\Pi_2$,$v'=2$ and $^3\Pi_1$,$v'=2$ showed that direct transfer to $^3\Pi_2$,$v'=1$ and $^3\Pi_1$,$v'=1$, respectively, must be included in the model. Furthermore, for excitation of $^3\Pi_2$,$v'=2$, emission always was observed from $^3\Pi_0$,$v'=3$, which indicates that the $^3\Pi_0$,$v' \leftrightarrow ^3\Pi_2$,$v'-1$ process must be important. In principle, the vibrational relaxation model for the $v'=2$ level has five rate constants, the three $^3\Pi_i(2) \rightarrow ^3\Pi_i(1)$ rate constants plus the $^3\Pi_0(2) \rightarrow ^3\Pi_2(1)$ and $^3\Pi_2(2) \rightarrow ^3\Pi_0(3)$ rate constants, that need to be assigned. As a starting point, we set the three $\Delta\Omega=0$ rate constants to be identical, and the other two rate constants were allowed to vary. The values of the rate constants were assigned by comparing calculated and experimental integrated band intensities for $v' = 1$ and 0 following excitation to specific $^3\Pi_{0,1,2}$,$v'=2$ levels and by simulating waveforms for the growth of populations in $v' = 1$ and 0 (see Figure 6c). The correct radiative branching rates[14] were included in calculating the

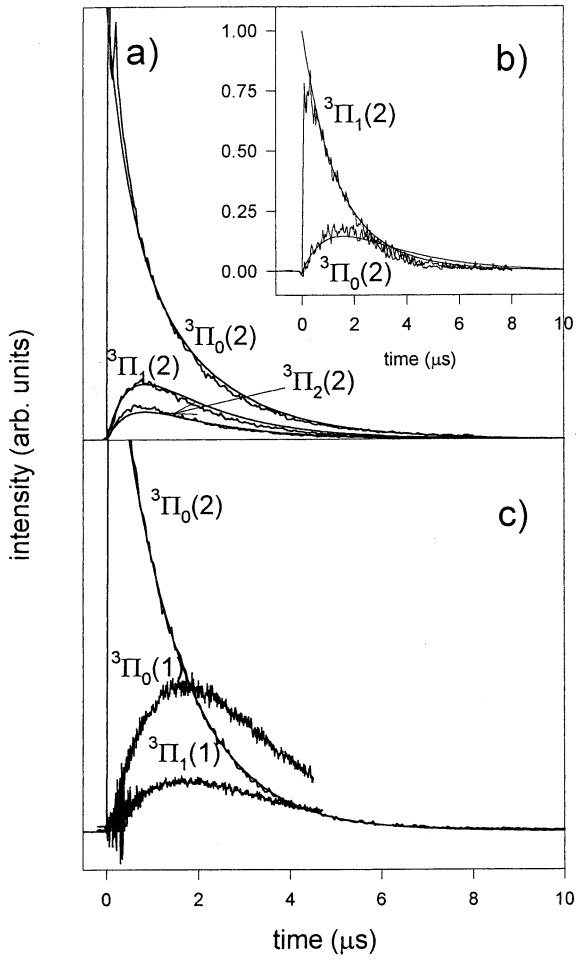


**Figure 6.** Waveforms illustrating the assignment of spin−orbit and vibrational relaxation rate constants for PF($A^3\Pi_{2,1,0},v'=2$) in He. The smooth curves are calculated decay plots. (a) Excitation of PF($^3\Pi_0,v'=2$) in 3 Torr with observation of the growth of concentrations in the $^3\Pi_1$, $v'=2$ and $^3\Pi_2,v'=2$ levels. (b) Excitation of PF($^3\Pi_1,v'=2$) in 1 Torr of He with observation of the growth of concentration in the $^3\Pi_0,v'=2$ level. (c) Excitation of PF($^3\Pi_0,v'=2$) in 4 Torr of He with observation of the growth of concentrations in the $^3\Pi_0,v'=1$ and $^3\Pi_1,v'=1$ levels. The rapid rise in the $^3\Pi_0,v'=1$ concentration identifies direct transfer from the $^3\Pi_0,v'=2$ level. The $^3\Pi_1,v'=1$ concentration is mainly formed by the two-step collisional cascade $^3\Pi_0,v'=2 \rightarrow {}^3\Pi_2,v'=1$ followed by $^3\Pi_2,v'=1 \rightarrow {}^3\Pi_1,v'=1$. These data were acquired in the same experiments as the data for the spectrum in Figure 3.

relative band intensities for the $v'$ and $v'-1$ levels. The data from excitation of $^3\Pi_2(v'=3)$ also was used to fit k($^3\Pi_0(3) \rightarrow {}^3\Pi_2(2)$). The best values are $k(^3\Pi_i(2) \rightarrow {}^3\Pi_i(1)) = k(^3\Pi_0(2) \rightarrow {}^3\Pi_2(1)) = 1.4 \times 10^{-12}$ and $k(^3\Pi_2(2) - {}^3\Pi_0(3)) = 1.0 \times 10^{-12}$ cm$^3$ s$^{-1}$; the total vibrational rate constants for the three individual Ω levels become $k(^3\Pi_2(2)) = 2.4 \times 10^{-12}$, $k(^3\Pi_1(2)) = 1.4 \times 10^{-12}$, and $k(^3\Pi_0(2)) = 2.8 \times 10^{-12}$ cm$^3$ s$^{-1}$. These values are consistent with $k^{He}_{vib}(2)$ in Table 1. Within the uncertainty of the fitting of the data, the ratio, $R$, of $k(^3\Pi_0(2) - {}^3\Pi_2(1))/k(^3\Pi_i(2) - {}^3\Pi_i(1))$ was unity.

The spectra acquired for observation of the $^3\Pi_{0,1,2},v'=1$ populations from excitations of $v'=2$ levels, also showed emission from $v'=0$ levels. Thus, we were able to assign a numerical value of $0.90 \times 10^{-12}$ for k($^3\Pi_i(1) \rightarrow {}^3\Pi_i(0)$) with the assumption that $R = k(^3\Pi_0(1) \rightarrow {}^3\Pi_2(0))/k(^3\Pi_i(1) - {}^3\Pi_i(0)) = 1$. Analysis of waveforms and relative intensity ratios for excitation of $^3\Pi_{0,1,2},v' = 3$ levels with observation of growth of populations in the $^3\Pi_{0,1,2},v'=2$ levels gave $k(^3\Pi_i(3) - {}^3\Pi_i(2)) = 2.1 \times 10^{-12}$ cm$^3$ s$^{-1}$. The $k(^3\Pi_1(4) - {}^3\Pi_1(3))$ value was estimated from $k_{tot}$He(4). Estimation of uncertainties in the vibrational relaxation model must include the value of $R$, as well the values for $k(^3\Pi_i(v) - {}^3\Pi_i(v-1))$. The value of $R$ could be changed by 20%, but not by 40%, in fitting the data. We estimate a ±30% uncertainty for the He rate constants of Table 3.

**TABLE 3: State-Resolved Vibrational Relaxation Rate Constants**[a]

| vibrational level | He[b] $\Delta\Omega = 0$ | Ar[c] $\Delta\Omega = 0$ |
|---|---|---|
| 1 | 0.9[e] | 0.6[d] |
| 2 | 1.4 | 1.4 |
| 3 | 1.9[f] | |
| 4 | 2.1[g] | 1.7 |
| 5 | | 2.7 |

[a] In units of $10^{-12}$ cm$^3$ molecule$^{-1}$ s$^{-1}$; see text for an estimate of uncertainties. [b] The ratio $k(^3\Pi_0(v') - {}^3\Pi_2(v'-1))/k(^3\Pi_i(v') - {}^3\Pi_i(v'-1))$ was equal to 1.0. [c] The ratio $k(^3\Pi_0(v') - {}^3\Pi_2(v'-1))/k(^3\Pi_i(v') - {}^3\Pi_i(v'-1))$ was equal to 2.0. [d] Assigned from $k_{vib}^{Ar}$ reported in ref 9. [e] Assigned in this work; however, the result agrees with $k_{vib}^{He}$ measured in ref 9. [f] Assigned from the $k^{He}_{vib}(3)$ value in Table 1 plus intensity ratios at 1 and 4 Torr from excitation of $^3\Pi_0(v'=3)$. [g] Estimated from the $k_{vib}^{He}(4)$ value in Table 1.

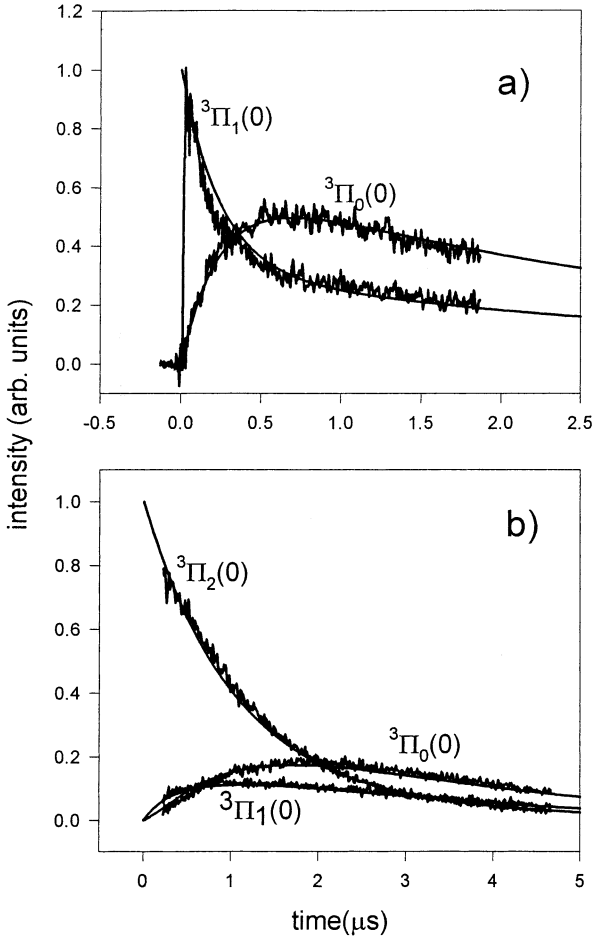


**Figure 7.** Waveforms for the excitation of (a) PF ($A^3\Pi_1,v'=0$) and (b) PF($^3\Pi_2,v'=0$) in 1.0 Torr of Ar. The smooth curves are the simulated results. Note the much faster decay rate of $^3\Pi_1,v'=0$ than for $^3\Pi_2,v'=0$.

**B.2. Spin−Orbit and State-Resolved Vibrational Relaxation Rate Constants in Ar.** The first step was to review the previous assignment[9] of the spin−orbit relaxation rate constants for $v'=0$. Spectra, such as those shown in Figure 12 of ref 9, and waveforms for selective excitation of the $^3\Pi_{0,1,2}$ levels, such as shown in Figure 7, were acquired[14] and fitted to obtain the improved rate constants (∼15% uncertainty) that are listed in

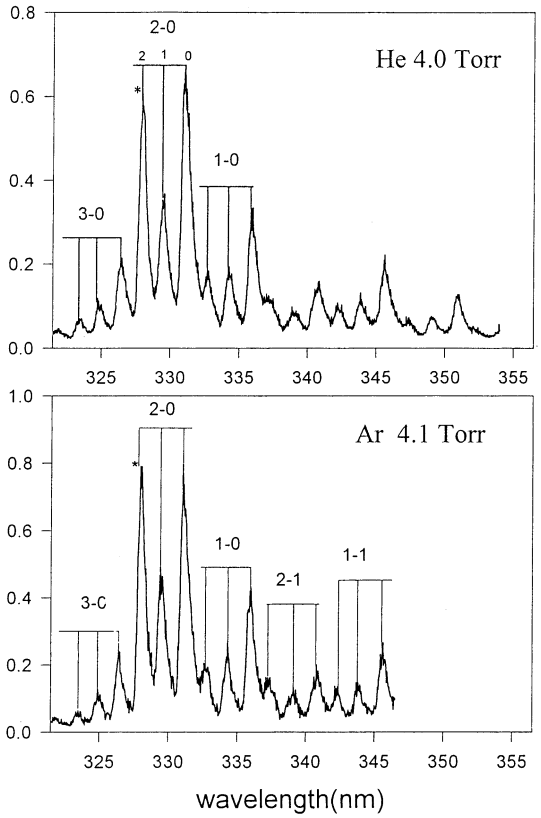


**Figure 8.** Comparison of integrated fluorescence spectra in 4 Torr of He and Ar following excitation of PF ($A^3\Pi_2$ ,$v'$=2). The nearly identical spectra suggest that the overall spin−orbit and vibrational relaxation rates for $^3\Pi_2$,$v'$=2 must be similar in He and Ar. However, time-resolved measurements, see text, identify significant differences in mechanism.

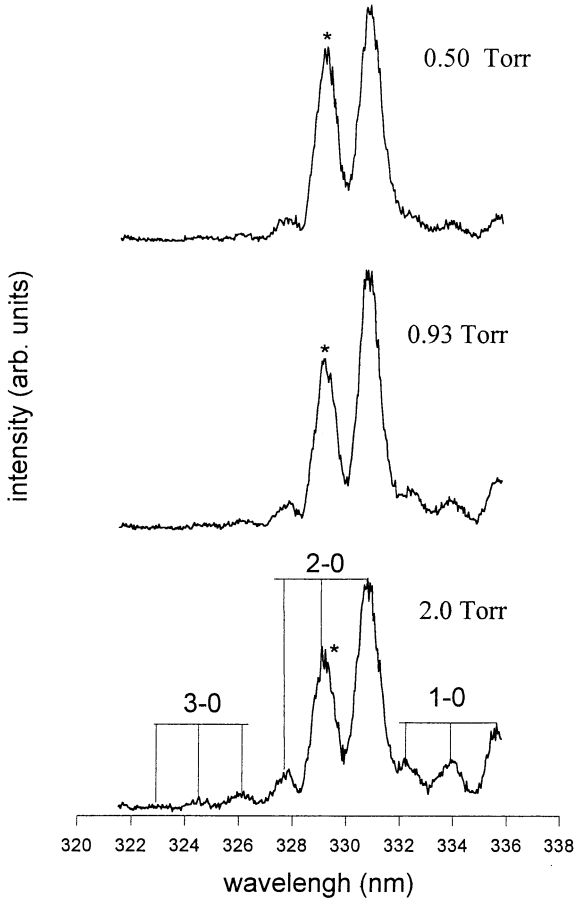


**Figure 9.** Comparison of fluorescence spectra from the PF($A^3\Pi_{0,1,2}$,$v'$=2) levels following excitation to the $A^3\Pi_1$ level for three pressures of Ar. Note the rapid transfer rate to $^3\Pi_0$,$v'$=2 (the $^3\Pi_0$ and $^3\Pi_1$ populations are in near equilibrium at 0.93 Torr.) but the slow transfer rate to $^3\Pi_2$,$v'$=2 and to $^3\Pi_1$,$v'$=1.

Table 2. The previously assigned[9] value for $k_{2,0}$ and $k_{2,1}$ were confirmed; however, the value for $k_{1,0}$ previously had been seriously underestimated. The fact that $k_{1,0}$ is significantly larger than $k_{2,1}+k_{2,0}$ is clearly evident from the waveforms of Figure 7b. The error can be traced to an analysis based on data acquired at too high a pressure.[9] A reliable value of $k_{1,0}$ only can be obtained from spectra for which collisional coupling of the populations in the $^3\Pi_0$ and $^3\Pi_1$ states occurs on a time scale comparable to the radiative lifetime, and not on a significantly shorter scale, as happens at higher pressures. Another experimental problem, which was not recognized,[9] was clipping of the fluorescence signal by the digitizer in some of the acquired waveforms. Several tests were made in the present work from experiments with pressures ≤1.5 Torr, and the $k_{1,0}$ = (8.0 ± 1.2) × $10^{-12}$ $cm^3$ $s^{-1}$ value should be firmly established. The rapid equilibration of the populations in the $^3\Pi_0$ and $^3\Pi_1$ levels makes analysis of the vibrational relaxation mechanism in Ar difficult. In the paragraphs that follow, analysis of the data for $v'$ = 2 and 4 is described in some detail. The total vibrational relaxation rate constant measured in ref 9 for $v'$=1 was used to estimate the value for $k(^3\Pi_i(1)\rightarrow{}^3\Pi_i(0))$ given in Table 3.

The fluorescence spectra from excitation of PF($A^3\Pi_2$,$v'$=2) in 4 Torr of He and Ar are compared in Figure 8. The degree of spin−orbit and vibrational relaxation seems to be comparable in the two cases, and the overall relaxation rate constants for $^3\Pi_2$,$v'$=2 must be similar in He and Ar. However, this is a case for which caution must be exercised in assignment of mechanisms for other Ω levels because, if the $v'$=2 case is like $v'$=0, the $^3\Pi_0$ and $^3\Pi_1$ state populations will be fully coupled at 4 Torr. The spectra in Figure 9 obtained from excitation of $^3\Pi_1$ in Ar clearly show that the transfer rate between the $^3\Pi_1$ and $^3\Pi_0$ levels is very rapid and much faster than transfer from either of these levels to $^3\Pi_2$. Some vibrational relaxation also is evident in the 0.93 and 2.0 Torr spectra. A detailed analysis of the pressure dependence of the relative band intensities and the waveforms following selective excitation of $^3\Pi_{0,1,2}$,$v'$=2 levels gave the same values, to within the combined experimental uncertainties, of $k_{2,1}$, $k_{2,0}$, and $k_{1,0}$ that were found for $v'$=0. However, a slightly better fit was found for $k_{1,0}$ = 6 × $10^{-11}$ rather than 8 × $10^{-11}$ $cm^3$ $s^{-1}$. Analysis of the data for excitation of $v'$=4 gave spin−orbit relaxation rate constants similar to those for $v'$=0. The much faster mixing of the $^3\Pi_{0,1}$ levels, relative to the transfer rate out of $^3\Pi_2$, is evident from the spectra for excitation of $v'$=4 in Figure 10. Limited experiments for $v'$=5 also gave a large value for $k_{1,0}$. In summary, for all of the $v'$ levels studied, $k_{1,0}$ seemed to be a factor of 5 larger than $k_{2,1}$.

Extensive data were acquired for excitation of $v'$ = 2 and 4 to study vibrational relaxation. The overall $k^{Ar}_{vib}$ ($v'$ = 2 and 4) was measured as 3.1 × $10^{-11}$ and >3.9 × $10^{-11}$ $cm^3$ $s^{-1}$ (Table 1); these Boltzmann weighted averages are dominated by $k(^3\Pi_0(v') - {}^3\Pi_0(v'-1)) + k(^3\Pi_0(v') - {}^3\Pi_2(v'-1))$. We began the more detailed analysis by assuming that $R$=1. However, inspection of the 0.5−1.0 Torr data for excitation of $^3\Pi_0$,$v'$=2 showed that more population was entering the $^3\Pi_2(1)$ level than $^3\Pi_0(1)$ level. The fast mixing between the $^3\Pi_1$ and $^3\Pi_0$ levels for both $v'$=2 and 1 precludes gaining any additional insight from excitation of $^3\Pi_1(v'=2)$. However, excitation of $^3\Pi_2(2)$ indicated that the growth of population in the $^3\Pi_0(3)$ state was

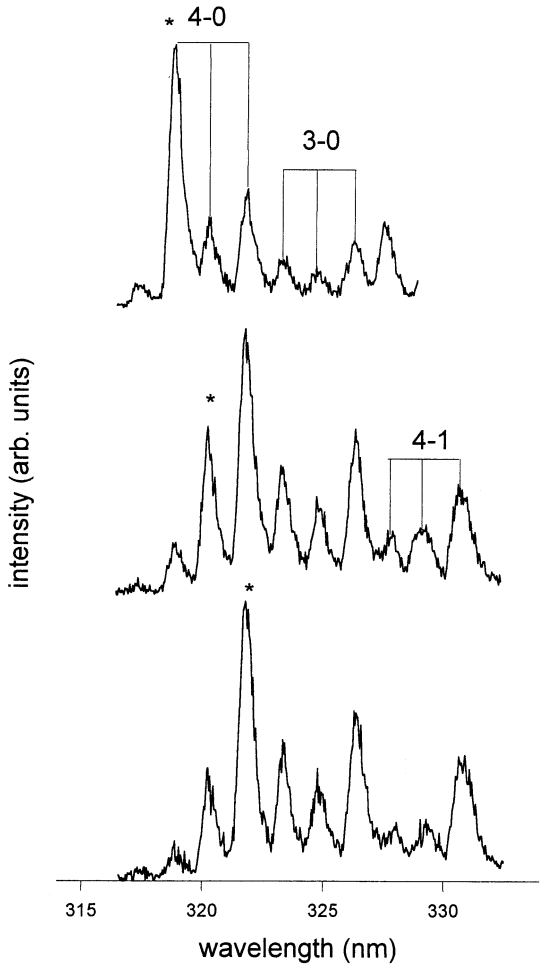


**Figure 10.** Comparison of fluorescence spectra for excitation of PF($A^3\Pi_{0,1,2}$,$v'$=4) levels in 1.5 Torr of Ar. Note the much more rapid relaxation following excitation of the $^3\Pi_0$ and $^3\Pi_1$ concentrations (lower and middle spectra) relative to the relaxation following excitation of the $^3\Pi_2$ concentration (upper spectrum).

comparable to the transfer to $^3\Pi_2(1)$. The data were finally fitted with $R\sim2$ and $k(^3\Pi_i(2) - {}^3\Pi_i(1)) = 1.4 \times 10^{-12}$ cm$^3$ s$^{-1}$. The pattern for relaxation from $v'$=4 seems to be the same as for $v'$=2, as can be observed by inspection of Figure 10. The degree of vibrational relaxation to $v'$=3 is much less for excitation of $^3\Pi_2$,$v'$=4 than for excitation of $^3\Pi_1$,$v'$=4 or $^3\Pi_0$,$v'$=4 for the same pressure of Ar. Furthermore, the $^3\Pi_2$,$v'$=3 emission band is greatly enhanced for excitation of $^3\Pi_1$ or $^3\Pi_0$, which shows that $R>1$. The $v'$=4 data were fitted by $R$=2 and $k(^3\Pi_i(4) - {}^3\Pi_i(3)) = 1.7 \times 10^{-12}$ cm$^3$ s$^{-1}$. The limited data acquired for $v'$=5 in Ar showed that the vibrational relaxation mechanism was similar to that for $v' = 2$ and 4. The degree of relaxation in 3 Torr of Ar was 2-fold greater than for relaxation in 4 Torr of He following excitation of $^3\Pi_1$,$v'$=5, which is consistent with the larger $k^{Ar}_{vib}$ in Table 1. Accessing the uncertainty in $R$ and $k(^3\Pi_i(v') - {}^3\Pi_i(v'-1))$ is difficult for $v' = 2$, 4, and 5. However, it is clear that $R$ is larger for Ar than for He, but that the $k(^3\Pi_i(v') - k(^3\Pi_i(v'-1))$ values are comparable in He and Ar.

## Discussion

The radiative lifetimes of PF($A^3\Pi_{0,1,2}$) molecules are independent of $\Omega$, but decline from 4.2 ± 0.2 to 1.8 ± 0.1 $\mu$s for $v'$=0−5. The variation of the lifetimes with vibrational level agrees with spectroscopic band-intensity data.[13] The band intensities and radiative lifetimes fit a transition-dipole funtion that declines with increasing $\langle r_{v',v''}\rangle$. The present work has provided improved values for $k_{2,0}$, $k_{2,1}$, and $k_{1,0}$ for relaxation of PF($A^3\Pi_{0,1,2}$,$v'$=0) by He and Ar, which were first reported in ref 9, plus new measurements for higher vibrational levels, up to $v'$=4 in He and $v' = 5$ in Ar. The values of the spin−orbit relaxation rate constants are independent of vibrational level; however, the individual rate constants are different for Ar vs He. The rate constants for $\Delta\Omega=-1$ changes are larger for Ar than for He; however, the rate constant for $\Delta\Omega=-2$ change is actually a factor of 2 smaller for Ar than for He. Thus, the sums of $k^{He}_{2,1}+k^{He}_{2,0}$ and $k^{Ar}_{2,1}+k^{Ar}_{2,0}$ have about the same values. However, because of the difference in reduced mass, the cross sections will differ by a factor of 2.5. The $\Delta\Omega=-1$ processes for $^3\Pi_2$ and $^3\Pi_1$ differ with $k_{1,0}$ being the larger by factors of ∼2 for He and ∼6 for Ar. A model was developed that included the spin−orbit states to interpret the vibrational relaxation rates for He and Ar. The minimum number of $\Delta v=-1$ pathways are the three $^3\Pi_i(v')\rightarrow{}^3\Pi_i(v'-1)$ processes plus the $^3\Pi_0(v')\rightarrow{}^3\Pi_2(v'-1)$ step. The $\Delta v=+1$ rate for $^3\Pi_2(v')\rightarrow{}^3\Pi_0(v'+1)$ also is needed to describe the overall vibrational relaxation of the population in a given $v'$ level. The $k(^3\Pi_i(v')\rightarrow{}^3\Pi_i(v'-1))$ values are similar in both He and Ar, but the $k(^3\Pi_0(v')\rightarrow{}^3\Pi_2(v'-1))$ value is 2 times larger in Ar than that in He. The present data for PF($A^3\Pi$) provide a reliable set of rate constants for the spin−orbit and vibrational relaxation for a $^3\Pi$ molecule with Hund's case (a) coupling. The need to explicitly include the spin−orbit states in the vibrational relaxation mechanism may be more general than previously recognized for $^3\Pi_{2,1,0}$ molecules with large spin−orbit energies.

According to the propensity rule based upon a first-order perturbation treatment,[16] $k_{2,0} > k_{2,1} \approx k_{1,0}$ for a $^3\Pi_{2,1,0}$ state with Hund's case (a) coupling.[17−19] In fact, for PF(A), $k_{2,0}/k_{2,1}\approx2$ and $k_{1,0}/k_{2,1}\approx2$ in He and $k_{2,0}/k_{2,1}=0.5$ and $k_{1,0}/k_{2,1}\approx6$ in Ar, and the propensity rule has limited utility. A similar conclusion was reached for the spin−orbit relaxation rate constant for SO($A^3\Pi_{0,1,2}$) in He and Ar. Since some of the results for SO(A) are not readily accessible, a summary is given below for easy comparison to the PF(A) results. Case (a) coupling is valid for the thermally populated ($N\leq35$) range of rotational levels of both PF($A^3\Pi$) and SO($A^3\Pi$), and the failure of the predicted propensity rule regarding the difficulty for $\Delta\Omega=\pm1$ changes cannot be attributed to the onset of Hund's case (b) coupling for the higher rotational levels.

The relaxation of SO($A^3\Pi$) $v' = 0$[6a] and 1[6b] in Ar was studied in considerable detail following excitation of each of the three $\Omega$ states. The assigned rate constants in Ar for $\Delta\Omega=-1$ change are $k_{2,1} = (1.6 \pm 0.8) \times 10^{-11}$ and $(2.0 \pm 0.5) \times 10^{-11}$; $k_{1,0} = (3.2 \pm 1.0) \times 10^{-11}$ and $(5.5 \pm 0.5) \times 10^{-11}$ cm$^3$ s$^{-1}$ for $v' =$ 0 and 1, respectively. Those data were fitted without a $^3\Pi_2\rightarrow{}^3\Pi_0$ rate; certainly $k_{2,0}$ is smaller than $k_{2,1}$. McAuliffe et al.[7] reported effective rate constants for spin−orbit relaxation following excitation of $^3\Pi_1(v' = 0$ and 1) that are somewhat smaller than Lo's value for $k_{1,0}$. Their kinetic analysis, which did not include reversible steps, could lead to an underestimate of $k_{1,0}$, and they concluded that the two sets of experiments were in agreement. McAuliffe et al. also reported results for experiments in He, and the $\Delta\Omega=-1$ rate constants based on $^3\Pi_1(v' = 0$ and 1) excitation were $(1.2 \pm 0.5) \times 10^{-11}$ and $(1.\ 0 \pm 0.3) \times 10^{-11}$ cm$^3$ s$^{-1}$, respectively, which are, on average, 1.5 times smaller than their results for Ar. Qualitative observations from excitation of $^3\Pi_1$ and $^3\Pi_0(v'=0)$ in He by Lo[6b] favor rate constants that are about 2-fold smaller than in Ar. Thus, both studies agree that the $\Delta\Omega=-1$ rate constants are smaller in He than Ar. Spectra[6b] from excitation of $^3\Pi_1$ in He suggest that $k_{1,0}$ *probably*

is larger than $k_{2,1}$. Unfortunately, no reliable data exist for excitation of $^3\Pi_2$ in He. On the basis on excitation of $^3\Pi_0$ with observation of formation of $^3\Pi_2$, the $k_{2,0}$ rate constant must be no larger than the $k_{1,0}$ rate constant. The vibrational relaxation of SO($A^3\Pi$),$v'=1$ has been interpreted as being dominated by the $^3\Pi_0(v'=1)\rightarrow{}^3\Pi_2(v'=0)$ step.[6] To within the experimental uncertainty, McAuliffe found the vibrational relaxation rate constants in He and Ar were the same,[7] $\sim 4 \times 10^{-12}$ cm$^3$ s$^{-1}$; however, Lo[6b] favors a somewhat larger rate constant ($7.5 \pm 1.5) \times 10^{-12}$ cm$^3$ s$^{-1}$ for Ar.[6d] Based on these limited data, the $\Delta v'=-1$, $\Delta\Omega=0$ pathways seem less important for SO(A,$v'$) than those for PF(A,$v'$).

Since the rotational relaxation rate with conservation of fine structure level (e.g., without spin−orbit relaxation) is the fastest relaxation process, the present work provides no information about the microscopic details of the intial and final rotational states of PF(A) in the $\Delta\Omega \geq -1$ or $-2$ processes. However, many of these details are available[18] for He interacting with PH($A^3\Pi_{2,1,0}$;$v'=0$); the naive molecular-orbital configuration is $\sigma^1\pi^3$, which has an inverted ordering of the spin−orbit states ($A=-116$ cm$^{-1}$). State-resolved product formation from excitation of $N'=1-6$ was reported. The spin−orbit rate constants for the nearly pure case (a) coupled levels of PH(A), $N' \leq 3$, are approximately five times larger than those for PF(A). The $\Delta\Omega=\pm1$ and $\Delta\Omega=\pm2$ rate constants were largest for transfer with small change in rotational state, i.e., $\Delta N' = 0$ and $\pm1$. The rate constants associated with $\Delta\Omega=+1$ change increased from $\sim 5 \times 10^{-11}$ to $12 \times 10^{-11}$cm$^3$ s$^{-1}$ for $N'=1-6$, and they became comparable to those for $\Delta\Omega=0$, $\Delta N'=\pm1$ processes for $N' \geq 4$, i.e., the spin−orbit state changing rates became comparable to the purely rotational relaxation rates. The increase in the rate constant for $\Delta\Omega=+1$ change seems to follow the degree of mixing between the case (a) basis functions, which grows with increasing $N'$.[18] In contrast, the rate constants for $\Delta\Omega=+2$, which are $\simeq 5 \times 10^{-11}$ cm$^3$ s$^{-1}$, are independent of $N'$. The calculated, for $N'=3$, theoretical cross sections[18] for $\Delta\Omega=+2$ changes also are 3−4 times smaller than for $\Delta\Omega=+1$ changes; the fractional contribution[18] of case (a) wave functions for $N'=3$ is about 90%. At least for He interacting with PH(A), the $\Delta\Omega = \pm1$ and $\pm2$ processes seem to occur with small changes in rotational state. This may be applicable to PF(A), but the much higher range of N′ for PF(A) than for PH(A) must be remembered in making this comparison. The PH(A) + He collisions certainly do not exhibit the predicted propensity for smaller cross sections for $\Delta\Omega=\pm1$ change than for $\Delta\Omega=\pm2$ change in either the experimental or theoretical results.[18]

Since the vibrational frequencies of PF(A) and IF($B^3\Pi_{0+}$) are similar, 436 and 411 cm$^{-1}$ respectively, their vibrational relaxation rate constants can be compared. The relaxation of IF(B,$v'=3$) has been studied in He, Ne, Ar, and Kr, and $v'=1-8$ have been studied in He.[20] The relaxation mechanism is direct and does not involve any intermediate electronic state of IF, and the relaxation cross sections changed with reduced mass as expected for vibrational-to-translational energy transfer according to the SSH theory. The collision cross-sections in He for IF(B,$v'=2$), 0.31 Å$^2$, and for PF(A,$v'=2$), 0.11 Å$^2$, differ by a factor of 3. The cross section for IF(B,$v'=3$) in Ar, 0.26, Å$^2$, is a factor of 2 smaller than that for He. On the other hand, the cross section for PF(A,$v'=2$) in Ar, 0.27 Å$^2$, is a factor of 2.5 *larger* than for He. In both He and Ar, the PF(A) comparison is for the $^3\Pi_i(2)\rightarrow{}^3\Pi_i(1)$ process. The SSH theory, which describes V−T transfer as a consequence of interactions on the repulsive part of the intermolecular potential, predicts that the cross section in Ar should be smaller than for He. Therefore, the assumptions of the SSH theory seem not to be applicable to Ar + PF(A,$v'$) interactions. The $^3\Pi_0(v')\rightarrow{}^3\Pi_2(v'-1)$ process that is important for both PF(A) and SO(A) requires more advanced models than V−T transfer. Presumably the smaller energy defect, relative to the $^3\Pi_2(v')\rightarrow{}^3\Pi_0(v')$ process, partly compensates for the change in $v'$ quantum number, since the rate constant for the $\Delta v=-1$, $\Delta\Omega=+2$ process is approximately equal and five times smaller than for the $\Delta v=0$, $\Delta\Omega=-2$ process in Ar and He, respectively.

As the final point, we will focus on the large $k_{1,0}$ value in Ar, which corresponds to a 16−20 Å$^2$ cross section and is within a factor of 3−4 of the gas kinetic limit. This experimental result suggests that the potentials for the Ar−PF($A^3\Pi_0$) and Ar−PF($^3\Pi_1$) pair differ from those of Ar−PF($A^3\Pi_1$) and Ar−PF($A^3\Pi_2$). Additional evidence for something special about the Ar−PF($^3\Pi_0$) potential is the enhanced $k(^3\Pi_0(v')\rightarrow{}^3\Pi_2(v'-1))$ rate constant in Ar. Support of this idea can be inferred from the spectroscopic data, which show that the PF($^3\Pi_0$, e levels) and the PF($^3\Pi_1$, e and f levels) states are homogeneously perturbed by the PF($b^1\Sigma^+$) and PF($d^1\Pi$) states, respectively.[13,21] Perhaps, additional mixing of PF electronic states occurs during the collisional interaction of Ar with PF($^3\Pi_0$ and $^3\Pi_1$), but not with PF($^3\Pi_2$). We will focus on the possible consequences of the mixing of $A^3\Pi_0$ (e levels) with the $b^1\Sigma^+$ state on the interaction potentials. Unlike NH($A^3\Pi$),[22] localized perturbations of the PF($A^3\Pi$) rotational levels do not seem to exist and gateway-mediated mechanisms need not be considered.

The interaction potentials for He or Ar with singlet or triplet $\Pi$ state diatomic molecules have A′ and A″ components when the spin contributions are ignored.[23,24] For PH($A^3\Pi$), the $V_{A''}$ component is the more repulsive one because the filled $\pi$ orbital is in the plane containing the three atoms, whereas for $V_{A'}$ the half-filled orbital is in the plane.[18,23,25] Since PF(A) has the $3\sigma^2 1\pi^4 2\pi^{*1} 4\sigma^{*1}$ configuration, the $V_{A'}$ and $V_{A''}$ potentials correspond to interaction with half-filled orbitals in both cases. Presumably, $V_{A'}$ is the more repulsive, but the $V_{A'}$ and $V_{A''}$ may be more similar than for the PH(A) example. The sum, $V_+$, and difference, $V_-$, of the $V_{A'}$ and $V_{A''}$ potentials actually are needed to describe the collisional processes, and $V_-$ is considered to be responsible for collision-induced change of populations between the spin−orbit states.[16,23,24] The PF($d^1\Pi$) state has the same molecular orbital description as PF($A^3\Pi$) and, to a first approximation, adding a PF(d) component to the PF($A^3\Pi_1$) state would not alter the relative positions of $V_{A'}$ and $V_{A''}$. However, the $b^1\Sigma^+$ state ($\sigma^2\pi^4\pi^{*2}$) has only an A′ potential. At least for the interaction of NH(b) with Ar, the $V_{b,A'}$ differs from the $V_{X,A''}$.[26] We would expect the Ar−PF($b^1\Sigma^+$) interaction to be more attractive than the Ar−PF($A^3\Pi_0$) interaction. Because of mixing of the b and A states, the Ar−PF($^3\Pi_0$(A′)) potential may differ from the A′ potentials associated with the $^3\Pi_1$ and $^3\Pi_2$ states. Relatively small changes in $V_{A'}$ can alter the difference potential, $V_-$, and affect the collisional coupling between the $^3\Pi_1$ and $^3\Pi_0$ levels. A more attractive potential for Ar−PF($^3\Pi_0$) than for He−PF($A^3\Pi_0$) also would help to explain the greater importance of the $^3\Pi_0(v')-{}^3\Pi_2(v'-1)$ pathway in Ar vs He. Recent state-resolved studies with CN($A^2\Pi$) have demonstrated that remarkably different relaxation mechanisms exist for Ar vs He collisions.[27]

## Conclusions

The radiative lifetimes of PF($A^3\Pi_{0,1,2}$) decrease from 4.2 to 1.8 $\mu$s from $v' = 0$ to 5. This decrease has been explained by a transition-dipole function that declines with increasing $\langle r_{v',v''}\rangle$.[14,21]

The relaxation mechanism and rate constants for spin−orbit relaxation at 300 K in He and Ar have been assigned for

$PF(A^3\Pi_{0,1,2})$ molecules, which follow Hund's case (a) coupling of spin and orbital angular momentum. Following pulsed laser excitation to a given state, rotational relaxation proceeds with conservation of $\Omega$, and the assigned spin−orbit relaxation rate constants are for a 300 K distribution of rotational states. For a specific bath gas, the mechanism and rate constants are independent of vibrational level up to $v'=5$. Both $\Delta\Omega = -1$ and $-2$ processes occur with the $\Delta\Omega=-1$ rate constants being larger in Ar than in He. Somewhat surprising, the rate constants for transfer of population between the $^3\Pi_1$ and $^3\Pi_0$ levels are larger than those for transfer between the $^3\Pi_2$ and $^3\Pi_1$ levels, even though both involve $\Delta\Omega=-1$ change. These experimental results do not support the propensity rules based on first-order perturbation theory for spin−orbit changing rates of case (a) coupled $^3\Pi$ molecules.

Vibrational relaxation proceeds by $\Delta v=-1$ changes with conservation of the $\Omega$ state, as well as with changes in $\Omega$ so as to minimize the energy defect, i.e., $PF(^3\Pi_0(v'))$+He or Ar giving $PF(^3\Pi_2(v'-1))$ must be included in the mechanism. The vibrational relaxation rates are about 5 times slower than those for spin−orbit relaxation. The cross sections for vibrational relaxation by Ar are larger than those for He in contrast to the expectation for a normal vibrational-to-translational energy transfer process. This result, plus the ease for collisionally induced $\Delta\Omega=\pm1$ changes, suggest that the attractive part of one or more of the interaction potentials between $PF(^3\Pi_{0,1,2})$ and Ar are stronger than expected from purely electrostatic interactions.

**Acknowledgment.** This work was supported by the National Science Foundation of the United States, Grant CHE 9505032.

## References and Notes

(1) Heaven, M. C. In *Chemical Dynamics in Extreme Environments*; Dressler, R., Ed.; World Scientific: Singapore, 2001.

(2) Henshaw, T. L.; Manke, G. C., II; Madden, T. J.; Berman, M. R.; Hager, G. D. *Chem. Phys. Lett.* **2000**, *325*, 537.

(3) McDermott, W. E.; Pchelkin, N. R.; Benard, D. J.; Bousek, R. R. *Appl. Phys. Lett.* **1978**, *32*, 469.

(4) (a) Malins, R. J.; Setser, D. W. *J. Phys. Chem.* **1981**, *85*, 1342. (b) Habdas, J.; Wategaonkar, S.; Setser, D. W. *J. Phys. Chem.* **1987**, *91*, 451.

(5) Manke, G. C., II; Setser, D. W. *J. Phys. Chem. A* **1998**, *102*, 7257.

(6) (a) Lo, G.; Beaman, R.: Setser, D. W. *Chem. Phys. Lett.* **1988**, *149*, 384. (b) Lo, G. Ph.D. Thesis, Kansas State University, Manhattan, Kansas, 1989, and unpublished data for He.

(7) McAuliffe, M. J.; Bohn, M.; Dorko, E. A. *Chem. Phys. Lett.* **1990**, *167*, 27.

(8) Stuart, B. C.; Cameron, S. M.; Powell, H. T. *J. Phys. Chem.* **1994**, *98*, 11499.

(9) Xu, J.; Setser, D. W.; Hamman, R. *J. Phys. Chem.* **1995**, *99*, 3173.

(10) Zhao, Y.; Setser, D. W. *J. Phys. Chem.* **1995**, *99*, 12179; *J. Phys. Chem.* **1994**, *98*, 9723.

(11) (a) Rengarajan, R.; Liu, C. P.; Setser, D. W. Unpublished work. (b) Attempts to use the H + $PF_2$ reaction, with $PF_2$ generated from the H + $PF_2Cl$ or $PF_2Br$ reactions, as a chemical source of $PF(a^1\Delta)$ molecules in a flow reactor were only partly successful.[11a] The product branching fractions of both the primary and secondary reactions needs further study. On the basis of the HCl(v) and HBr(v) infrared chemiluminescence data, it seems as if H atom addition to the phosphorous atom competes with Cl and Br atom abstraction in the H + $PF_2Cl$, $PF_2Br$, and $PBr_3$ reactions.[11c] (c) Rengarajan, R. M.S. Thesis, Kansas State University, Manhattan, Kansas, 1995.

(12) Zhao, Y.; Setser, D. W. *J. Chem. Soc., Faraday Trans.* **1995**, *91*, 2979.

(13) Nizamov, B.; Setser, D. W. *J. Mol. Spectrosc.* **2001**, *206*, 53.

(14) Nizamov, B. Ph.D. Thesis, Kansas State University, Manhattan, Kansas, 1999.

(15) Drabbels, M.; Wodtke, A. M. *J. Chem. Phys.* **1998**, *109*, 355.

(16) Alexander, M. H. *Chem. Phys.* **1985**, *92*, 337 and earlier papers mentioned here.

(17) (a) Dagdigian, P. J. In *The Chemical Dynamics and Kinetics of Small Radicals*; Liu, K., Wagner, W., Eds.; World Scientific: Singapore, 1995; Part 1. (b) Dagdigian, P. J. *Annu. Rev. Phys. Chem.* **1997**, *48*, 95.

(18) Neitsch, L.; Stuhl, F.; Dagdigian, P. J.; Alexander, M. H. *J. Chem. Phys.* **1997**, *106*, 7642.

(19) Neitsch, L.; Stuhl, F.; Dagdigian, P. J.; Alexander, M. H. *J. Chem. Phys.* **1996**, *104*, 1325.

(20) Wolf, P. J.; Davis, S. J. *J. Chem. Phys.* **1987**, *87*, 3492.

(21) Fitzpatrick, J. A. J.; Chekhov, O. V.; Elks, J. M. F.; Western, C. M.; Ashworth, S. H. *J. Chem. Phys.* **2001**, *115*, 6920.

(22) Mo, Y.; Ottinger, C.; Shen, G. *J. Chem. Phys.* **1999**, *111*, 4598.

(23) Kolczewski, C.; Fink, K.; Staemmler, V.; Neitsch, L. *J. Chem. Phys.* **1997**, *106*, 7637.

(24) Pouilly, B.; Dagdigian, P. J.; Alexander, M. H. *J. Chem. Phys.* **1987**, *87*, 7118.

(25) Jonas, R.; Staemmler, V. Z. *Phys. D.* **1989**, *14*, 143.

(26) Jansen, G.; Hess, B. A. *Chem. Phys. Lett.* **1992**, *192*, 21.

(27) Nizamov, B.; Dagdigan, P. J.; Alexander, M. H. *J. Chem. Phys.* **2001**, *115*, 8393.